J Solid State Electrochem (2009) 13:1025–1036
DOI 10.1007/s10008-009-0823-4

ORIGINAL PAPER

Carbon modified (CM)-n-TiO_2 thin films for efficient water splitting to H_2 and O_2 under xenon lamp light and natural sunlight illuminations

Yasser A. Shaban · Shahed U. M. Khan

Received: 9 August 2008 / Revised: 25 February 2009 / Accepted: 4 March 2009 / Published online: 3 April 2009

Abstract Visible light-active carbon modified n-type titanium oxide (CM-n-TiO_2) thin films were synthesized by both flame oxidation and a combination of spray pyrolysis and flame oxidation. An undoped reference sample was also synthesized in an electric oven for comparison. Photoresponse of CM-n-TiO_2 and n-TiO_2 was evaluated by measuring the rates of water splitting to hydrogen and oxygen, in terms of observed photocurrent densities. Under monochromatic illumination from a xenon lamp, the integrated photocurrent densities from 300 nm to wavelengths corresponding to band gaps were found to be 1.12, 7.7, and 12.7 mA cm^{-2} for optimized oven-made n-TiO_2 (sample 1), flame-made (sample 2), and spray pyrolysis flame-made CM-n-TiO_2 (sample 3) thin films at 0.48, 0.24, and 0.215 V biases, respectively. The corresponding maximum photoconversion efficiencies for these thin films were 0.84%, 7.62%, and 12.89%, respectively. Under actual natural global AM 1.5 sunlight illumination of 1 sun, the photocurrent densities for water splitting were 0.85, 5.89, and 12.27 mA cm^{-2} for samples 1, 2, and 3, respectively. These photocurrent densities generated the maximum photoconversion efficiencies of 0.67%, 5.63%, and 12.26% for samples 1, 2, and 3, respectively, under global sunlight illuminations. These values compared well with those found under monochromatic light illumination from the xenon lamp. The increasing efficiencies were found to be consistent with lowering of main band gap from 3.0 eV to 2.65 eV and the generation of mid-gap bands at 1.6 eV and 1.4 eV above the valence band for samples 2 and 3, respectively. Carbon contents were found to be 0.0, 17.60, and 23.23 atom% for samples 1, 2, and 3, respectively.

Keywords CM-n-TiO_2 thin films · Water splitting · Sunlight · Illumination

Introduction

Sunlight can ultimately become an unlimited source of clean and renewable energy if it could be harnessed efficiently to split water to hydrogen and oxygen. Numerous studies have focused on semiconductor photoelectrodes for their applications in water-splitting reactions [1–22]. Most of these studies sought highly stable and low-cost semiconductor materials for efficiently harvesting solar energy. Among the photoelectrode materials investigated, titanium dioxide (n-TiO_2) was recognized to be the most promising because of its low cost, chemical inertness, nontoxicity, and photostability. However, its wide band gap (3.0–3.2 eV) limits its photoresponse in the ultraviolet region, which is only a small fraction (~5%) of the sun's energy compared to visible light from 400 to 750 nm (~49%). Hence, any shift in the optical response of n-TiO_2 from the UV to the visible spectral range will have a profound positive effect on the photocatalytic efficiency of the material. Several attempts were made to lower the band gap of n-type titanium oxide (n-TiO_2) by transition metal dopants [23, 24], but no noticeable change in band gap energy of n-TiO_2 was observed. Visible light absorption by the transition metal-doped n-TiO_2 was found to be due to *d–d* transition of electrons in the transition metal dopants, not for band gap lowering. The transition metal dopants had an adverse effect in the photocatalytic activity of n-TiO_2

Dedicated to the 85th birthday of John O' M. Bockris.

Y. A. Shaban · S. U. M. Khan (✉)
Department of Chemistry and Biochemistry, Duquesne University, Pittsburgh, PA 15282, USA
e-mail: khan@duq.edu

because they acted as recombination centers for the photogenerated carriers.

However, recent studies have involved doping of n-TiO_2 by carbon [1, 15–22, 25–30], nitrogen [31, 32], and sulfur [33], as well as fabricating carbon-modified n-type titanium oxide (CM-n-TiO_2) in mesoporous [34, 35] and nanostructure [36, 37] forms. Photocatalytic activity of sulfur-doped n-TiO_2 was found to diminish under UV and visible light illuminations due to catalytic poisoning induced by oxidation of sulfur to SO_2 and SO_4^{2-}. Photocatalytic activity of nitrogen-doped n-TiO_2 for the degradation of organics was reported to be much lower than carbon-doped n-TiO_2 [30]. However, no studies on photosplitting of water by nitrogen-doped n-TiO_2 were reported as yet.

It was found that carbon modification of n-TiO_2 photocatalysts synthesized by thermal oxidation of Ti metal in a natural gas flame lowered the band gap energy of n-TiO_2 to 2.32 eV and exhibited water splitting to hydrogen and oxygen with a photoconversion efficiency of 8.35% [1] under artificial light from a xenon lamp. This progress stimulated further investigation into carbon modified n-TiO_2 (CM-n-TiO_2) as visible light active photocatalysts [25–30] and as photoelectrodes [15–22] for water splitting reactions with enhanced photoconversion efficiency.

Sakthivel and Kisch [30] observed visible light absorption by carbon-doped n-TiO_2 nanoparticles synthesized by hydrolysis of $TiCl_4$ with tetrabutylammonium hydroxide ($C_{16}H_{36}NOH$) followed by calcinations of the precipitates. They observed a fivefold increase in photocatalytic activity of carbon-doped n-TiO_2 as compared to those that had been nitrogen-doped. Irie et al. [25] observed a visible light response for carbon-doped n-TiO_2 synthesized by partial oxidation of titanium carbide powder. Xu et al. [28] reported that the carbon-modified n-TiO_2 nanoparticles, synthesized by a wet process using a glucose ($C_6H_{12}O_6$) solution as the carbon source, absorbed well into the visible light spectrum to near-infrared region up to 800 nm. These CM-n-TiO_2 samples showed a 13-fold increase in photocatalytic activity as compared to regular undoped n-TiO_2 due to band gap lowering from 3.2 to 2.78 eV and the generation of a mid-gap band at 1.45 eV above the valence band.

Importantly, Mohaputra et al. [18] synthesized CM-n-TiO_2 thin films by flame oxidation of Ti metal sheets and reported a photoconversion efficiency of 8.5% for water splitting, which is slightly higher than earlier results [1]. Carbon doping was considered to be responsible for the lowering of the band gap of n-TiO_2 and consequent high photocatalytic activity under visible light illumination. Noworyta and Augustynski [19] observed shifts in the spectral response (up to 425 nm) during water-splitting reactions for carbon-doped n-TiO_2 film electrodes formed in the flame of a burner fed with various gas mixtures. Shanker et al. [38] investigated the effect of flame annealing on the spectral photoresponse of titania nanotubes and demonstrated the enhancement of the visible light absorption and the photocurrent for water splitting due to annealing in the flame. Xu et al. [39, 40] prepared highly ordered n-TiO_2 nanotube array films by electrochemical anodization of Ti metal sheet followed by calcinations in an electric oven and further oxidation in natural gas flame to incorporate carbon into n-TiO_2 films. Significant enhancement of the photoresponse of these CM-n-TiO_2 nanotube films for water splitting also was reported [39, 40].

Hahn et al. [41] prepared carbon-doped, self-organized n-TiO_2 nanotube layers formed by electrochemical anodization of Ti in a HF/Na_2HPO_4 electrolyte. The tubes were treated at 500°C under a mixed flux of N_2 and acetylene (C_2H_2). The acetylene-treated carbon-doped nanotubes showed a significant photoresponse over the entire range of visible light up to the near-IR region (827 nm). Nakano et al. [42] prepared TiO_2/C films by oxidative annealing of sputtered TiC films. They reported three bands having energies 0.86, 1.30, and 2.34 eV below the conduction band of carbon-doped n-TiO_2. They attributed the 0.86 eV level to the intrinsic nature of TiO_2, whereas the 1.30 and the 2.34 eV levels were newly introduced by C-doping and behaved as deep-level bands. In particular, the pronounced 2.34 eV band contributed to band gap narrowing by mixing C 2*p* with the O 2*p* valence bands. Therefore, the 2.34 eV level played a significant role for the visible-light sensitivity in TiO_2/C. Ren et al. [43] synthesized a visible-light-active TiO_2 photocatalyst by carbon doping using glucose as a carbon source via a hydrothermal method at temperatures as low as 160 °C. Recently, carbon-modified n-type titanium oxide (CM-n-TiO_2) photoelectrodes synthesized by thermal flame oxidation of Ti metal sheets were found to split water with a maximum photoconversion efficiency of 9.02% [20], which exhibited a significant shift in spectral response up to 775 nm. Importantly, an optimized CM-n-TiO_2 sample synthesized on grooved surface [21] generated a maximum photoconversion efficiency of 7.62% for water splitting at an applied potential of 0.242 V under actual sunlight illuminations of global AM 1.5 (1 sun).

In an important theoretical study, Nie and Sohlberg [44] reported the lowering of the band gap of n-TiO_2 to 2.32 eV (535 nm) due to carbon incorporation and predicted that the band gap value of 1.58 eV may be possible to achieve by some complex carbon doping. Interestingly, it was found experimentally that enhanced carbon doping lowered the band gap of n-TiO_2 to 1.45 eV [16]. Wang and Lewis [45, 46] theoretically addressed the effects of carbon dopants concentration on the photoresponse of n-TiO_2 in the visible-light region. They found that the substitutional and interstitial carbon dopants incorporated into TiO_2 drastically affected the electronic structure of the material, thus improving its photoactivity. They predicted the low-band

gap of 2.35 eV for carbon-doped TiO_2 as it was experimentally observed earlier [1]. The theoretical findings of Valentin et al. [47] revealed the presence of substitutional and interstitial carbon in CM-n-TiO_2, which were found to be responsible for the lowering of its main band gap as well as generating a mid-gap band.

In the present study, we focused on enhancing the photoconversion efficiency for the water splitting reaction at CM-n-TiO_2 thin film electrodes synthesized by using a combination of both spray pyrolysis and thermal flame oxidation methods. The results of these samples were compared to those synthesized using only thermal flame oxidation and also with reference unmodified n-TiO_2 synthesized by thermal oxidation in an electric oven. The carbon content in CM-n-TiO_2 was identified by energy dispersive spectroscopy (EDS). The surface characterization of CM-n-TiO_2 photoelectrodes was performed by employing a scanning electron microscopic (SEM) analysis. The photoresponse and the photoconversion efficiency for water splitting at CM-n-TiO_2 photoelectrodes were determined under both white light and monochromatic light illumination from a 150-W xenon arc lamp and also under actual global sunlight illumination of AM 1.5 (1 sun).

Experimental details

Synthesis of reference n-TiO_2 films in an electric oven (oven-made)

Titanium (0.25 mm thick, 99.5% from Alfa Co.) metal sheets were cut, cleaned in a sonicator for three 15-min intervals with (1) acetone, (2) acetone/double deionized water (1:1), and then with (3) double deionized water. After drying in air, these metal sheets were oxidized in an electric oven (Multiple Unit, Series C4497 WEO). A digital thermocouple [Thermolyne Corp K-type Thermocouple (PM-20700)] was used to measure and maintain the temperature of the oven. The oxidation temperature and oxidation times were varied from 800 to 950 °C and from 5 to 30 min, respectively.

Synthesis of CM-n-TiO_2 films by thermal flame oxidation method (flame-made)

Titanium (0.25 mm thick, 99.5% from Alfa Co) metal sheets were cut to an area of ~1.0 cm^2. Ti metal samples were cleaned as described in Section on Synthesis of reference n-TiO_2 films in an electric oven (oven-made). After air drying, these metal sheets were thermally oxidized by using a custom-designed large flame (Knight, Model RN 3.5x a WC) under controlled natural gas and oxygen flows. Most importantly, the flame must be kept facing downward to minimize the excess air flow from the surroundings. The oxidation temperature and the oxidation time were varied from 800 to 950 °C and from 5 to 30 min, respectively. Each flame oxidation temperature was kept constant for the duration of oxidation by controlling the flow rates of oxygen (1.5–2.0 L/min) and the natural gas (2.0 L/min). The flow rates of both natural gas and oxygen were measured using a flow meter (Omega Engineering, Model FL-1806). The digital thermocouple (Thermolyne Corp K-type Thermocouple, PM-20700) was used to measure and maintain the temperature of the flame. The oxide layers on the top of the front and back sides of the Ti samples were removed using a file. This area was used to make electric contact using a copper clip. The back side and part of the front side were covered with a non-conducting epoxy adhesive. The uncovered area of the photoelectrode, which was exposed to incident light, was calculated using an Image J computer program.

Synthesis of CM-n-TiO_2 films by the combination of spray pyrolysis and thermal flame oxidation (spray-flame made)

Spray pyrolytic synthesis of thin films of semiconductors was described earlier in detail [4, 7]. The spray solution consisted of 0.175 M $TiCl_4$ in ethanol. Titanium metal sheets from Alfa (0.25 mm thick, 99.5% pure) were used as substrates. A custom-made Pyrex 250 mL round-bottom flask with two spray attachments on the glassware was used to spray the solution. These attachments consisted of two burette-like tips positioned at a 90° angle. The lower burette serves to deliver the ethanolic solution, and the other burette tip acts as the point at which the carrier gas flows to atomize the ethanolic solution.

The spray pyrolysis was carried out at a substrate temperature of 460 °C for a total of 20 s. The pressure of the carrier gas (oxygen) was maintained at 20 psi. Five-minute breaks were allowed between each spray period of 10 s to maintain a constant temperature on the substrate surface. A Thermolyne Corp. K-type Thermocouple (PM20700, Series 405) was used to measure and maintain the temperature of Ti metal substrate placed on a Fisher Scientific hotplate. Thermal flame oxidation for 16 min at 825 °C (as described in Section on Synthesis of CM-n-TiO_2 films by flame oxidation (flame made)) was then performed.

Measurements of photocurrent density

The measurements of photocurrents were performed in a single compartment three-electrode photoelectrochemical cell using an oven-made n-TiO_2, flame-made CM-n-TiO_2, or spray-flame made CM-n-TiO_2 samples as the working electrode. Platinum net were used as a counter-electrode, and a saturated calomel electrode (SCE) was used as a reference electrode. An electrolyte solution of 5 M KOH was used in all such measurements. The surface of the

photoelectrodes was illuminated with light intensity of 100 mW cm^{-2} from a 150-W xenon arc lamp (Kratos Model LH 150/1). The spectral irradiance of white light and also wavelength-dependent monochromatic light from a 150-W xenon lamp were measured by using a silicon detector (UDT Sensors, Model 10DP/SB). The photocurrent, j_p, as a function of measured potential, E_{meas}, vs. SCE was determined using an EG & G Princeton Applied Research model 362 scanning potentiostat with scan rate of 50 mV/s and plotted using an EG & G Princeton Applied Research (Houston Model RE 0092) X–Y recorder. The photocurrent, j_p was obtained by subtracting dark current from current under illumination of light. A Keithley multimeter was used to measure the electrode potential at open circuit conditions before scanning each sample.

The photocurrents under monochromatic light illumination, j_p (λ), as a function of wavelength, λ, were measured using a 362 EC & G scanning potentiostat, a Spectra Physics monochromator, model 77250, and a Keithley multimeter.

UV-Vis spectroscopic measurements

UV-Vis absorption spectra of CM-n-TiO_2 and n-TiO_2 were recorded using a Varian Cary 1E UV-Visible Spectrophotometer with a Varian GRID 36is-25 microprocessor and a Dell Optiplex PC. Labsphere (Model DRA-Ca-30I) with a reflectance standard (I.D.USRS-99-010) was used. The UV-Vis absorption spectra were measured for the wavelength range between 190 and 800 nm by means of double reverse reflectance.

Scanning electron microscopic measurements

SEM were taken using a Zeiss EVO-SEM in which conductive carbon tape was used to make contact with the conductive titanium surface with the aluminum sample deck.

X-ray diffraction measurements

X-ray diffraction (XRD) data were collected using a PANalytical Xpert-Pro MPD X-ray diffractrometer. The scans, having angles from 18° to 70° (2θ), were carried out using a Cu Kα radiation (λ=1.544 Å) operating at 40 mA and 45 kV. Samples were run with a continuous scan at a rate of 0.100°/min with a recording period of 0.017°.

Energy dispersive spectroscopic measurements

An electron microprobe attached to the SEM unit (Model Cam Scan series 4) used in EDS mode was employed to obtain quantitative information of the amounts of carbon in CM-n-TiO_2. Furthermore, this EDS system did not use a carbon grid as a sample holder. The samples were placed directly on an aluminum sample deck. An X-ray detector with an ultrathin window was used to facilitate the detection of light elements like carbon. The EDS was performed using a Princeton Gamma Tech. Inc. Integrated Microanalyzer software package.

Results and discussion

Dependence of photocurrent density on measured electrode potential

Figure 1 shows the photocurrent density, j_p, as a function of measured potential, E_{meas} (V/SCE) under light intensity of 100 mW cm^{-2} from a 150-W xenon lamp for oven-made n-TiO_2 synthesized at the optimized temperature of 825 °C for the optimum time of 16 min (sample 1); CM-n-TiO_2 synthesized by only thermal flame oxidation of Ti at optimum 825 °C for an optimum 16 min (sample 2); CM-n-TiO_2 synthesized by spray pyrolysis of 0.175 M $TiCl_4$ in ethanol at the optimum substrate temperature of 460 °C for an optimum 20 s at carrier gas (oxygen) pressure of 20 psi; and then followed by flame oxidation at the optimum flame temperature of 825 °C for 16 min (sample 3).

Sample 1 exhibited the lowest photoresponse. The observed low photocurrent density at sample 1 can be

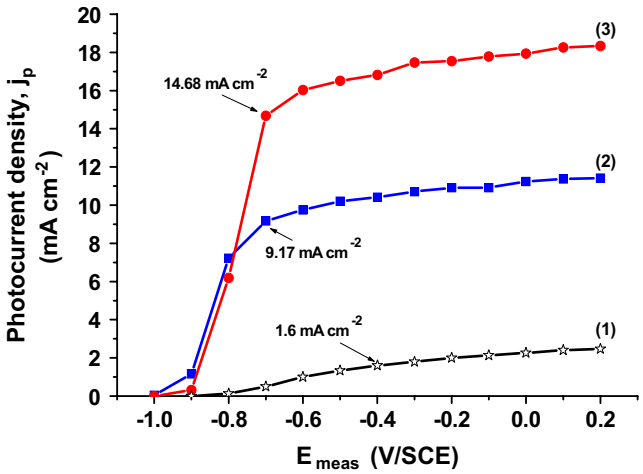

Fig. 1 Photocurrent density, j_p, as a function of measured potential, E_{meas} (V/SCE), at white light intensity of 100 mW cm^{-2} from a 150-W xenon lamp, for oven-made n-TiO_2 synthesized at 825 °C for 16 min (sample 1), CM-n-TiO_2 synthesized by only thermal flame oxidation of Ti at 825 °C for 16 min (sample 2), and CM-n-TiO_2 synthesized by a combination of spray pyrolysis of 0.175 M $TiCl_4$ in ethanol at a substrate temperature of 460 °C for 20 s at a carrier gas (oxygen) pressure of 20 psi followed by thermal flame oxidation at 825 °C for 16 min (sample 3); electrolyte solution of 5 M KOH was used

attributed to the absence of carbon incorporation during the oxidation of the Ti metal sheet in an electric oven and also to lower thickness TiO_2 layer formed. CM-n-TiO_2 photoelectrodes (sample 3) generated the highest photoresponse because of their low multiple band gaps and higher thickness. Photocurrent density, measured at −0.7 V/SCE and under white light illumination intensity of 100 mW cm^{-2} from the xenon lamp, increased significantly from 9.17 mA cm^{-2} for sample 2 to 14.68 mA cm^{-2} for sample 3 due to a higher thickness and lower mid-band gap values. These results clearly indicate that the spray pyrolysis process helped to enhance the absorption of light by increasing the thickness of CM-n-TiO_2 films. Consequently, higher photocurrent density was observed due to the absorption of more light in these thicker CM-n-TiO_2 films of lower band gap energies.

Dependence of photoconversion efficiency on applied potential

The calculation of total percent photoconversion efficiency [% ε_{photo} (total)] of light energy under white light illumination to chemical energy in the presence of an external applied potential (E_{app}) was carried out using the equation given earlier [1, 4] as

$$\%\,\varepsilon_{photo}(\text{total}) = \frac{j_p\left(E^{\phi}_{rev} - |E_{app}|\right)}{P_0} \times 100 \qquad (1)$$

where j_p is the photocurrent density (in mA cm^{-2}), E^{ϕ}_{rev} is the standard reversible potential (which is 1.23 V for the water splitting reaction), P_o is the power density of incident light (in mW cm^{-2}), and $|E_{app}|$ is the absolute value of the applied potential, E_{app}, which is obtained as [1],

$$E_{app} = (E_{means} - E_{aoc}) \qquad (2)$$

In this equation, E_{meas} (vs. SCE) is the potential at which the photocurrent density was measured, and E_{aoc} (vs. SCE) is the electrode potential at the open circuit condition in the same electrolyte solution under the same illumination intensity at which the photocurrent density was measured. The values of E_{aoc} (vs. SCE) were -0.847 V, - 0.940 V, and - 0.915 V for samples 1, 2, and 3, respectively.

The corresponding maximum photoconversion efficiencies (see Fig. 2) were 1.2% at 0.447 V bias, 9.08% at 0.240 V bias, and 14.04% at 0.215 V bias for samples 1, 2, and 3, respectively. However, due to enhancement of the thickness in sample 3, as well as the lowering of mid-band gap energy due to increased carbon incorporation, maximum photoconversion efficiency of 14.04% was observed at only 0.215 V bias under white light illumination from the xenon arc lamp.

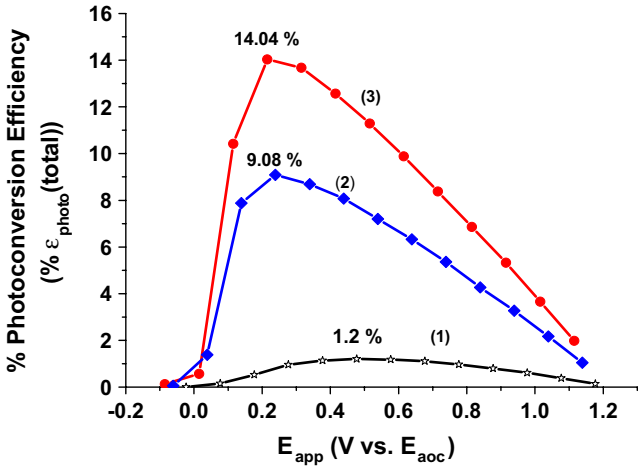

Fig. 2 Dependence of photoconversion efficiency,% ε_{photo}(total), on applied potential E_{app} (V vs. E_{aoc}), for samples 1, 2, and 3. The electrode potentials at open circuit conditions under illumination, E_{aoc}, were found to be −0.977 V/SCE, −0.940 V/SCE, and −0.915 V/SCE for samples 1, 2, and 3, respectively

Monochromatic photocurrent density - wavelength dependence

The monochromatic photocurrent densities, j_p (λ), as a function of wavelength of light, λ, for samples 1, 2 and 3 are shown in Fig. 3. The monochromatic photocurrent density, j_p (λ), was measured at the measured potential (corresponding to an applied potential at which maximum photoconversion efficiency% ε_{photo}(total) under white light illumination was observed). At the applied potentials, E_{app} of 0.477 V, 0.240 V and 0.215 V vs E_{aoc} were used to measure j_p (λ) under monochromatic light illumination for samples 1, 2, and 3 respectively.

Performing integration under the curves from 250 nm to 800 nm, total photocurrent densities of 1.25, 8.95 and 13.58 mA cm^{-2} were observed for samples 1, 2, and 3,

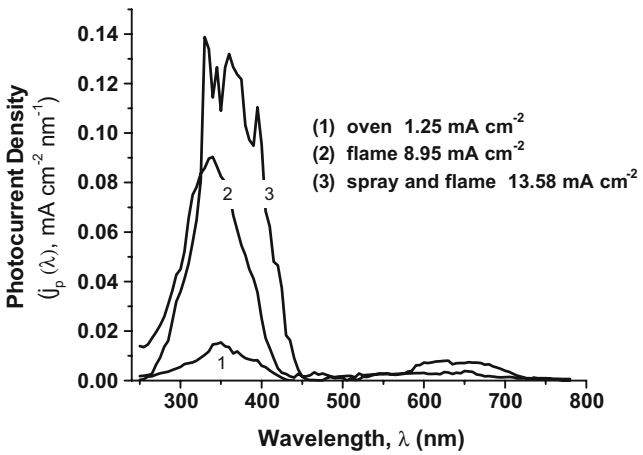

Fig. 3 The monochromatic photocurrent density, j_p (λ), as a function of wavelength of light, λ, for samples 1, 2, and 3

respectively. These values are a little lower than the corresponding photocurrent density values under white light illumination from the xenon lamp. Loss of some light when passing through the monochromator may be responsible for these lower values.

Photoconversion efficiency from monochromatic photocurrent density

Alternatively, the percent total photoconversion efficiency (% ε_{photo}(total)) of light energy to chemical energy can be obtained by using the following equation [20, 21, 48, 49]:

$$\%\,\varepsilon_{photo}(\text{total}) = \frac{\int_{\lambda_{min}}^{\lambda_g} j_p(\lambda)\left[E_{rev}^{\phi} - \left|E_{app}(\lambda)\right|\right]d\lambda}{\int_{\lambda_{min}}^{\infty} P_0(\lambda)d\lambda} \times 100 \quad (3)$$

where $j_p(\lambda)$ is the wavelength dependent photocurrent density under monochromatic light illumination (mA cm^{-2} nm^{-1}) and P_o (λ) is the power density of incident monochromatic light (mW cm^{-2} nm^{-1}). Note that the applied potential, E_{app} (λ) was found to be wavelength dependent and can be expressed as [21]

$$E_{app}(\lambda) = E_{means} - E_{aoc}(\lambda) \quad (4)$$

where E_{aoc} (λ) is the electrode potential in volts at open circuit conditions under monochromatic light illumination. The λ_{min}=250 nm for the light from the xenon lamp and 300 nm for sunlight and λ_g=1239.85/E_g is the threshold wavelength corresponding to band gap energy, E_g, of the sample in electron volt units.

Note that wavelength-dependent percent photoconversion efficiency, % ε_{photo} (λ) can be expressed as [20, 21]

$$\%\,\varepsilon_{photo}(\lambda) = \frac{j_p(\lambda)\left[E_{rev}^{\phi} - \left|E_{app}(\lambda)\right|\right]}{\int_{\lambda_{min}}^{\infty} P_0(\lambda)d\lambda} \times 100 \quad (5)$$

Using the j_p (λ) values given in Fig. 3, total power density of light in the denominator of Eq. 5 as 100 mW cm^{-2} and performing the integration (as given in Eq. 3) from λ_{min}= 250 nm (available in xenon lamp white light) to λ_g in nanometer or determining the area under the curve obtained using Eq. 5, total photoconversion efficiencies of 0.94%, 8.86%, and 13.79% were obtained for samples 1, 2, and 3, respectively. These efficiency values are little lower because of loss of light through the monochromator but compares well with those of 1.2%, 9.08%, and 14.04% obtained under white light illuminations.

It is observed in Fig. 3 that higher photocurrent response and consequent higher photoconversion efficiency of CM-TiO_2 samples was determined by the unusually higher ability of the material to use the absorbed UV photons to convert OH^- ions to O_2 gas. Such unusual behavior of CM-n-TiO_2 samples mainly in the UV regions may be explained in terms of following effects. One is the possible multi-electron-hole pairs (excitons) generation (MEG) by absorption of single high energy photons in the UV region across multiple low energy band gaps in the CM-n-TiO_2 nanocrystals (Ncs), as it is observed in its scanning electron microgram (see Fig. 9). The multi-exciton generation (MEG) by a single photon was observed earlier [51–53] in Ncs and explained theoretically in terms of impact ionization [54–56]. Such MEG by a single photon can be explained also by other physical process, such as generation of multiple excitons by absorption of light when excess energy of photogenerated electrons by high energy UV photons is lost as radiation.

Furthermore, the microscopic nanocrystalline, nanowall, and rough surface of CM-n-TiO_2 could have temporarily trapped microscopic oxygen gas bubbles that may have acted as tiny lenses and spherical mirrors that helped to concentrate the incident light on the electrode surface, augmenting the photoresponse for water splitting by an order of magnitude [57].

Band gap energy determination

The band gap energy, E_g, can be determined from the frequency of light, ν, dependent quantum efficiency, η (ν), using the following equation [4, 5, 7]:

$$\eta(\nu)h\upsilon = A\left(h\upsilon - E_g\right)^n \quad (6)$$

where A is a constant, n equals either 0.5 for allowed direct transition or 2 for allowed indirect transition, and $h\nu$ is the photon energy of frequency, ν. The wavelength, λ, dependent quantum efficiency, η (λ), or incident photon conversion efficiency IPCE (λ) can be expressed as [21, 49],

$$\eta(\lambda) = \text{IPCE}(\lambda) = \frac{j_p(\lambda)}{eI_0(\lambda)} = \frac{1,239.85\,\text{V nm}\,j_p(\lambda)[\text{mA cm}^{-2}\,\text{nm}^{-1}]}{\lambda\,nm\,P_0(\lambda)[\text{mW cm}^{-2}\text{nm}^{-1}]} \quad (7)$$

where e is the electronic charge and the wavelength dependent incident photon flux, I_o (λ) (cm^{-2} nm^{-1} s^{-1}) was expressed as [21, 49]

$$I_0(\lambda) = \frac{P_0(\lambda)\times\lambda}{hc} = \frac{P_0(\lambda)(\text{mW cm}^{-2}\text{nm}^{-1})\times\lambda\,\text{nm}}{1,239.85\,\text{V nm}\times e} \quad (8)$$

where h is the Planck's constant and c is the velocity of light.

Figure 4 shows $[\eta(\lambda)h\upsilon]^{1/2}$ vs. $h\upsilon$ plots for samples 1, 2, and 3. The band gaps were obtained from the intercepts of the straight lines. Two indirect band gap energies for CM-n-TiO_2 photoelectrodes are shown. The first band gap energy of 2.65 eV corresponds to a lowering of the original band

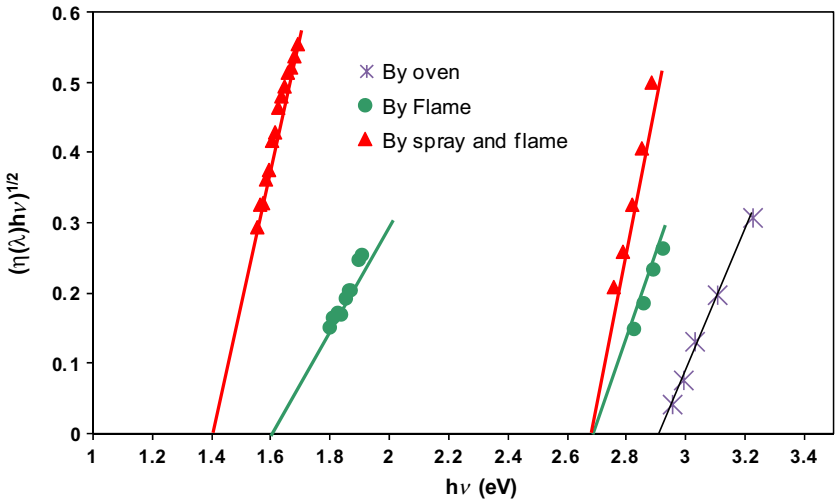

Fig. 4 The plots of $[\eta\ (h\upsilon)]^{1/2}$ vs. $h\upsilon$ to determine the band gap for sample 1, 2, and 3

gap (3.0 eV), and the second band gap with values of 1.4 eV (for sample 3) and 1.6 eV (for sample 2) can be attributed to mid-gap band generated by carbon doping (see Fig. 5). Theoretical analyses [44–47] and experimental findings [42] also showed multiple band gaps in CM-n-TiO_2. Oven-made n-TiO_2 showed only one band gap of 2.9 eV, and as a result, poor photoresponse was obtained. Note that the first band gap energy values for both CM-n-TiO_2 samples 2 and 3 were found to be equal. The slopes of band gap plots for sample 3 were found to be the highest, which is consistent with the highest observed photoresponse generated by this sample.

The theoretical studies [42–47] involving density of states calculations were carried out to determine the types of carbon present in CM-n-TiO_2 structure and explain the possible electronic structure in terms of band gap lowering and mid-gap band formation that conform with our experimentally determined values of band gaps and observed enhanced photocurrent response in these samples. These theoretical studies suggested the presence of substitutional carbon, which replaces oxygen, and also the interstitial carbon nearby an oxygen vacancy in CM-n-TiO_2. It was also suggested that the interstitial carbons were responsible for the generation of electronic states or bands in the gap and the substitutional carbons lowered the band gap as shown in Fig. 5.

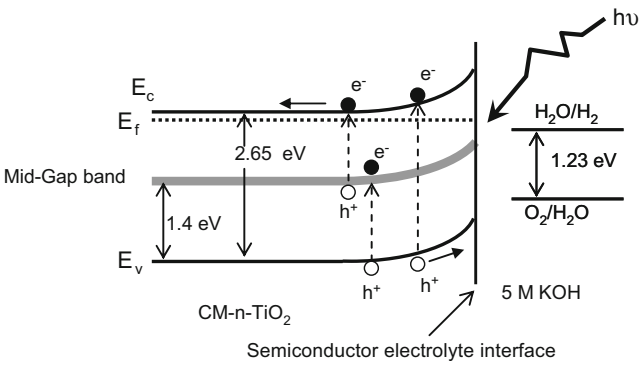

Fig. 5 A schematic diagram of valence, conduction, and mid-gap bands to show the band gaps in CM-n-TiO_2 films (sample 3). The energy levels of H_2O/H_2 and O_2/H_2O at CM-n-TiO_2 solution interface are shown also

Spectral distribution of AM 1.5 sunlight (1 sun) and xenon lamp light (100 mW cm^{-2})

It is important to compare the spectral distribution of light from both the xenon lamp and sunlight. Figure 6 compares the spectral distribution of these two lights. The integrated value of the intensity from 300 to 800 nm for global natural sunlight AM 1.5 (1 sun)=100 mW cm^{-2} measured by National Renewable Energy Laboratory (NREL) [50] was found to be 59.00 mW cm^{-2}; this clearly indicates that the contribution from the remaining light from 800 to 4,100 nm

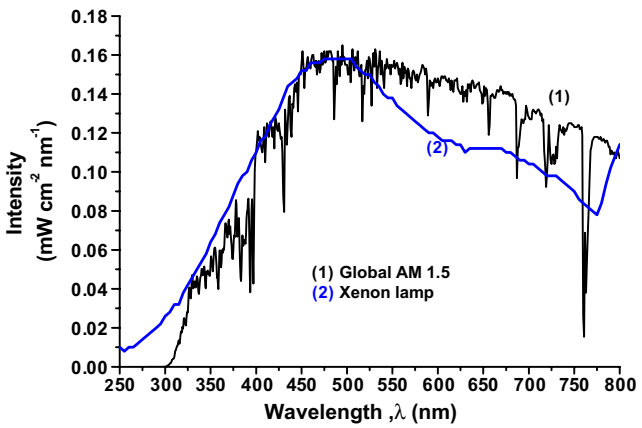

Fig. 6 The wavelength-dependent intensity of light from a 150-W xenon lamp at intensity of 100 mW cm^{-2}, measured by using a silicon photon detector (UDT Sensors, Model 10DP/SB), compared to the wavelength dependent intensity of natural global AM 1.5 sunlight in the wavelength range of 300 to 800 nm obtained from NREL website [50]

present in global sunlight will be 41.00 mW cm^{-2} [=(100–59)mW cm^{-2}]. Hence, total xenon lamp light comparable to sunlight (1 sun) will be 97 mW cm^{-2} [=(56+41)mW cm^{-2}] where 56.00 mW cm^{-2} is the integrated value of intensity from 200 to 800 nm for xenon lamp light.

Note that the spectral distribution of xenon lamp light begins below 250 nm (at 200 nm) compared to global AM 1.5 sunlight that begins at 300 nm. Furthermore, the spectral distribution of xenon lamp light is higher in the UV region, but in the visible region, it is lower than that of sunlight. Hence, one will expect comparable photocurrent density and photoconversion efficiencies for CM-n-TiO_2 samples for water splitting under actual global sunlight illumination of AM 1.5 (1 sun) and the xenon lamp illumination of intensity of 100 mW cm^{-2}. However, relatively, the higher values for photocurrent density and photoconversion efficiency under xenon lamp illumination will be expected as compared to those under sunlight for CM-TiO_2 due to the higher spectral distribution of the former in the UV region than in the visible region (see Fig. 7) and that the absorption coefficient of light of CM-TiO_2 in the UV region is much higher compared to that in the visible region (see Figs. 3 and 8).

Photocurrent density and photoconversion efficiency from IPCE (λ) under natural sunlight illuminations

Utilizing the values of the wavelength-dependent incident photon conversion efficiency, IPCE (λ), or quantum efficiency, η (λ), of the CM-n-TiO_2 samples, it is possible to determine the photocurrent density, j_p^{sunlight} (λ), under natural sunlight of global AM 1.5 as

$$j_p^{\text{sunlight}}(\lambda) = \text{IPCE}(\lambda)\, e\, I_0^{\text{sunlight}}(\lambda) \tag{9}$$

where $I_o^{\text{sunlight}}(\lambda)$ is the wavelength-dependent photon flux of incident global AM 1.5 sunlight, which can be obtained using Eq. 8, where the wavelength, λ, dependent photon power density P_o^{sunlight} (λ) was used from the tabulated data in the NREL web site [50].

The plots of $j_p^{\text{sunlight}}(\lambda)$ (data obtained from Eq. 9) vs. the wavelength of light, λ, for samples 1, 2, and 3 are given in Fig. 7. The integrated values of total current density under sunlight illumination from $\lambda_{\min}$=300 nm to λ_g were found to be 0.85, 5.85, and 12.27 mA cm^{-2} for samples 1, 2, and 3, respectively. For each wavelength of light, a fixed value of E_{app} (applied potential at which maximum photoconversion efficiency was observed under white light illumination) was used during the experiment by adjusting the E_{meas} values (see Eq. 4).

Similarly, the total photoconversion efficiency under natural sunlight illumination can be expressed using Eq. 10 as

$$\%\,\varepsilon_{\text{solar}}^{\text{sunlight}}(\text{total}) = \frac{\int_{\lambda_{\min}}^{\lambda_g} j_p^{\text{sunlight}}(\lambda)\left[E_{\text{rev}}^{\phi} - \left|E_{\text{app}}(\lambda)\right|\right]\mathrm{d}\lambda}{\int_{\lambda_{\min}}^{\infty} P_0^{\text{sunlight}}(\lambda)\mathrm{d}\lambda} \times 100 \tag{10}$$

where the denominator was taken as 100 mW cm^{-2} for actual natural global AM 1.5 sunlight (1 sun).

Hence, using Eq. 10, one gets its simplified form for the water splitting reaction (for which is E_{rev}^{ϕ} 1.23 V) as

$$\%\,\varepsilon_{\text{solar,total}}^{\text{sunlight}} = \frac{J_{\text{p,total}}^{\text{sunlight}}(\text{mA cm}^{-2}) \times \left(1.23\text{V} - E_{\text{app}}\text{V}\right)}{100(\text{mW cm}^{-2})} \times 100 \tag{11}$$

where

$$J_{\text{p,total}}^{\text{sunlight}} = \int_{\lambda_{\min}}^{\lambda_g} j_p^{\text{sunlight}}(\lambda)\mathrm{d}\lambda \tag{12}$$

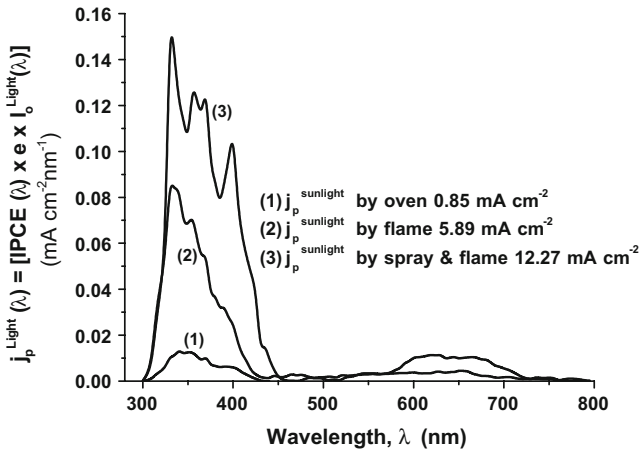

Fig. 7 Wavelength-dependent photocurrent density under natural global sunlight illumination, j_p^{sunlight} (λ) vs. wavelength, λ, of incident sunlight for samples 1, 2, and 3.

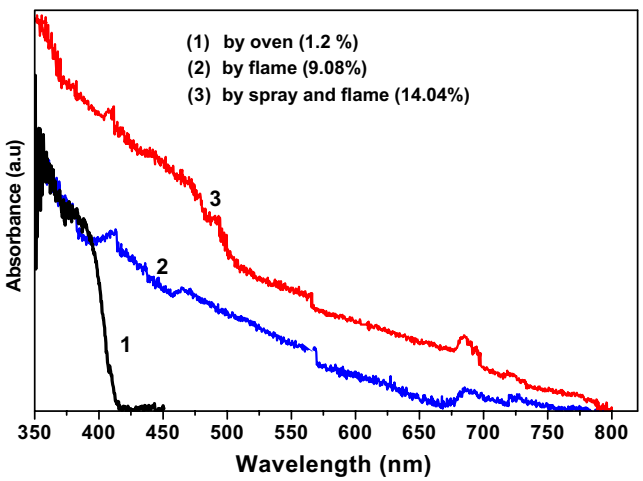

Fig. 8 UV-Visible spectra for electric oven-made n-TiO_2 for samples 1, 2, and 3

Table 1 Maximum photoconversion efficiencies (%) under xenon lamp light and actual natural sunlight illumination conditions for electric oven-made n-TiO_2 (sample 1), flame-made CM-n-TiO_2 (sample 2), and spray pyrolysis flame-made CM-n-TiO_2 (samples 3) and their band gap and mid-gap energies

Titanium oxide,TiO_2 samples	Percent maximum photoconversion efficiency under white light illumination from Xenon lamp light	Percent maximum Photoconversion efficiency under monochromatic light illuminations from xenon lamp		Percent maximum Photoconversion efficiency under monochromatic actual natural sunlight illuminations (integrated from 300nm present in sunlight to λ_g in nm)	Band gap energies	
		Integrated from 200nm to λ_g in nm	Integrated from 300nm to λ_g in nm		Band gap energy (eV)	Mid-gap energy (eV)
Oven-made (sample 1)	1.2	0.94	0.84	0.67	2.9	None
Flame-made (sample 2)	9.08	8.86	7.62	5.63	2.65	1.6
Flame-made on grooved Ti surface [21]	11.31	11.16	8.41	7.62	2.65	1.6
Spray pyrolysis and flame-made (sample 3)	14.04	13.79	12.89	12.26	2.65	1.4

Photoconversion efficiencies under sunlight illumination can be obtained using Eq. 10 or 11. The wavelength, λ, dependent percent photoconversion efficiencies can be obtained using in Eq. 5 under sunlight illumination as a function of wavelength of incident light, λ, for samples 1, 2, and 3. Performing the integration under the curve from 300 nm to λ_g in nanometer, photoconversion efficiencies of 0.67%, 5.63%, and 12.26% were found under actual natural sunlight illumination for samples 1, 2, and 3, respectively. Alternatively, using Eq. 12 in Eq. 11, the photoconversion efficiencies under sunlight illumination can be obtained also. These results indicate that CM-n-TiO_2 thin films synthesized by a combination of spray pyrolysis and natural gas flame oxidation (sample 3) can be expected to split water with ≥10% efficiency even under actual sunlight illumination. The photoconversion efficiency values under different experimental conditions are summarized in Table 1.

UV-Vis spectra

The UV-Vis absorbance of n-TiO_2 and CM-n-TiO_2 photoelectrodes is shown in Fig. 8. The absorption spectra of CM-n-TiO_2 samples 2 and 3 demonstrate a wide absorption in the UV and visible regions with a tail extending to the near-infrared region up to 800 nm. This indicates low-band gap energy values for these samples. The reference oven-made n-TiO_2 (sample 1) shows absorption only up to 415 nm, which corresponds to band gap energy of 3.0 eV. The low-band gaps of CM-n-TiO_2 samples may be due to carbon incorporation during the flame oxidation of the Ti metal sheet. The UV-Vis spectroscopic results show higher absorption in UV, as well as in the visible regions for CM-n-TiO_2 films synthesized by a combination of spray pyrolysis and flame oxidation (sample 3) compared to sample 2. Furthermore, these UV-Vis spectra are consistent with the higher photocurrent densities at the CM-n-TiO_2

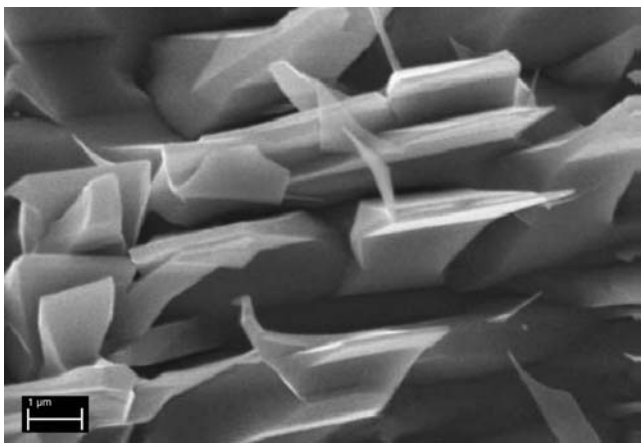

Fig. 9 SEM images for sample 3 in 1-μm scale

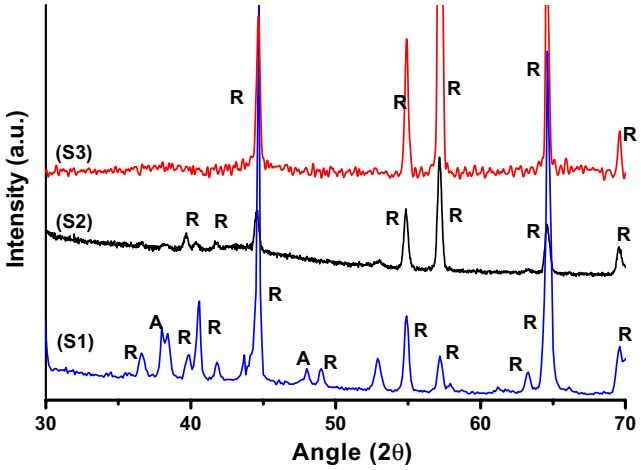

Fig. 10 X-ray diffraction (XRD) patterns for S1 (sample 1), S2 (sample 2) and S3 (sample 3)

thin film electrodes prepared by the combination of the two methods. Importantly, this observation conforms to the hypothesis that the spray pyrolysis increased the thickness of the visible light active CM-n-TiO_2 films. Consequently, these films absorbed more light.

However, the UV-Vis spectra (see Fig. 8) do not match well with the monochromatic photocurrent density-wavelength dependent plots (see Fig. 3). The UV-Vis spectra represent the excitation of electrons from a lower energy state (to generate holes in this state) to higher energy state by absorption of light. However, to have photocurrent, photo-generated holes will have to be (1) transported to the interface and (2) undergo transition across the interface to available (thermally distributed) hole acceptor states (e.g., OH^- ions) in solution. These two extra processes are responsible for the mismatch between the UV-Vis spectra and the monochromatic photocurrent density-wavelength dependent plots.

The electrons that are excited to conduction band from the shallow mid-gap band in CM-n-TiO_2 (see Fig. 5) by the light of wavelength around 500 nm shows absorption in the UV-Vis spectra. However, the holes generated in the mid-gap band (see Fig. 5) are lost by recombination due to very low availability of acceptor states of holes in solution. Consequently, negligible photocurrent density was generated (see Fig. 3). However, absorption of light in the UV-Vis spectra around 500 nm was observed because such absorption does not require the availability of acceptor states of holes in solution. Furthermore, the light around 500 nm (2.48 eV) having sub-band gap energy cannot be absorbed by CM-n-TiO_2 to generate electron-hole pairs in its valence band. However, the light around 600 to 700 nm can excite electrons from the valence band to mid-gap band states of CM-n-TiO_2 (see Fig. 6); these electrons move to the counter electrode. The corresponding holes generated in the valence band undergo transition to available acceptor states of holes in solution (OH^- ions). Consequently, some photocurrents are observed in this wavelength region (see Fig. 3).

Scanning electron microscopy

The surface characterization of CM-n-TiO_2 film (for sample 2) was performed by employing a SEM; the image is shown in Fig. 9. The surface appears to be extremely rough and composed of nanocrystals and nanowalls, thus providing much higher surface area to absorb incident light, multiple absorption and reflection to absorb more light, and contributed enhanced photoresponse.

X-ray diffraction

XRD measurements were carried out to characterize the structure of n-TiO_2 (sample 1) and CM-n-TiO_2 (samples 2 and 3). Figure 10 shows the XRD patterns for samples 1, 2, and 3. The peaks of these XRD spectra of both CM-n-TiO_2 photoelectrodes (S2 and S3) are consistent with the rutile structure. The XRD results demonstrate that the crystal structure of oven-made n-TiO_2 (S1) is a mixture of anatase and rutile forms. It is important to note that some peaks of the rutile structure are missing in both CM-n-TiO_2 samples (S2 and S3) compared to those in oven-made n-TiO_2 (S1).

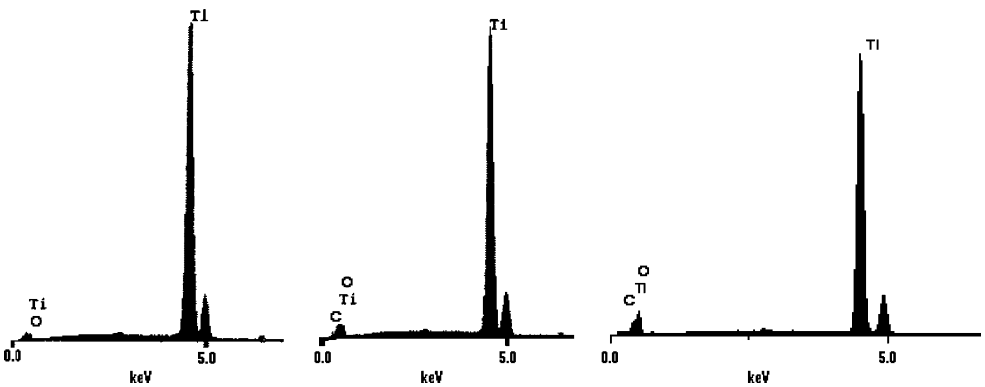

Fig. 11 Pattern of energy dispersive spectroscopy (EDS) of: **a** sample 1, **b** sample 2, and **c** sample 3

Table 2 Atom percent of elements Ti, O, and C in regular n-TiO_2 and CM-n-TiO_2 films from EDS data

Element	Atom%		
	Oven-made n-TiO_2	Flame made CM-n-TiO_2	Spray and flame made CM-n-iO_2
Ti	33.33	15.73	10.10
O	66.66	66.67	66.67
C	0.0	17.60	23.23

This indicates the marked influence of carbon modification on the structure of n-TiO_2.

Energy dispersive spectroscopy

Figure 11 shows the pattern of EDS for samples 1, 2, and 3. The presence of carbon in both CM-n-TiO_2 thin films (samples 2 and 3) and its absence in the electric oven-made reference n-TiO_2 (sample 1) was observed. The carbon contents increased significantly from 17.60 atom% for CM-n-TiO_2 synthesized using only thermal flame oxidation to 23.23 atom% for CM-n-TiO_2 synthesized by the combination of spray pyrolysis and thermal flame oxidation (see Table 1 for details). The increased photoconversion efficiencies for water-splitting reactions are consistent with increased atom% of carbon in the samples.

The results in Table 2 were obtained from EDS data, which are considered semi-quantitative. Furthermore, carbon atoms that may be present as substitutional, interstitial, and on the surface are all included in the EDS data. In addition, from powder X-ray data (see Fig. 10), one cannot identify the type of carbon (graphitic C, C_{60}, C_n, etc.) present in the sample. For such identification detail, XAFS and XANES studies must be carried out. Since all different types of carbon are included in the EDS data, it is not imperative that 50% of Ti has been replaced by carbon. Hence, the EDS data in Table 2 provides mainly qualitative information concerning the presence of carbon and its relative amounts in these three samples.

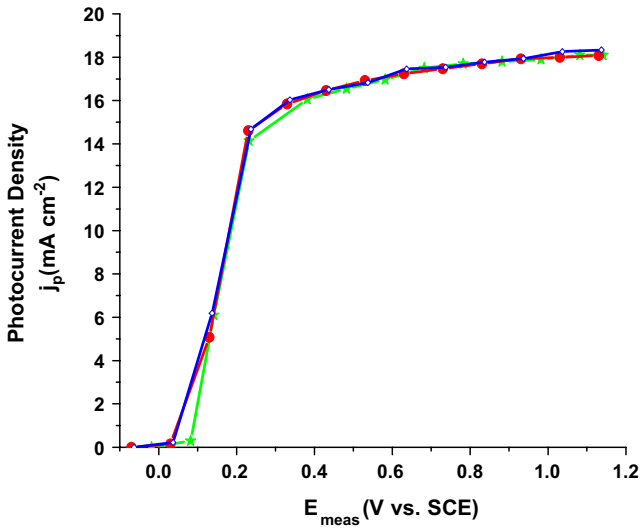

Fig. 12 Reproducibility test of CM-n-TiO_2 (sample 3) synthesized by combination of spray pyrolysis and flame oxidation in terms of photocurrent density. All three CM-n-TiO_2 thin film electrodes were prepared at the same optimum conditions used for sample 3. The electrode potentials at the open circuit condition under illumination, E_{aoc}, were found to be −0.915±0.02 V/SCE for all three films

Reproducibility of synthesis of CM-n-TiO_2

Reproducibility is one of the critical aspects of thin film fabrication. The reproducibility of the best performing CM-n-TiO_2 (sample 3) synthesized at the same optimum conditions was tested. Figure 12 shows photocurrent density, j_p, vs. $E_{meas,}$ the measured potential, V/SCE, of three CM-n-TiO_2 photoelectrodes synthesized by a combination of spray pyrolysis and thermal flame oxidation under the conditions of the synthesis of sample 3. At open circuit conditions, all three CM-n-TiO_2 samples were found to have almost the same value of E_{aoc}=−0.915±0.02 V vs. SCE under the same illumination conditions. The three samples demonstrate approximately consistent values of photocurrent densities at all measured potentials with standard deviation of 0.01 mA cm^{-2} at the potential at which photoconversion efficiency was found to be maximum.

Conclusions

It is essential to optimize the temperature and the time of both the spray pyrolysis and thermal flame oxidation processes to synthesize CM-n-TiO_2 films of highest photoconversion efficiency. Multiple exciton generation (MEG) by a single energetic photon [51–56] in UV region, across the mid-gap bands in the nanocrystalline CM-n-TiO_2, and incident photon concentrations [57] by the temporarily trapped oxygen gas bubbles on the nanowalls of CM-n-TiO_2 acting as tiny lenses and spherical mirrors helped to augment its photoresponse for water splitting reactions. The combination of the spray pyrolysis and flame oxidation process helped to increase the thickness of the CM-n-TiO_2 films, which facilitated the absorption of more light and consequently enhanced the photoresponse and the photoconversion efficiency to a considerable extent to 12.26% under actual natural sunlight illuminations (summarized in

Table 2). A correlation was found between the atom% of carbon content and the amount of visible light absorption to the consequently higher photoconversion efficiency.

Acknowledgment The authors gratefully acknowledge NETL/DOE for the financial support of this project.

References

1. Khan SUM, Al-Shahry M, Ingler WB Jr (2002) Science 297:2243
2. Licht S, Wang B, Mukerji S, Soga T, Umeno T, Tributsch H (2000) J Phys Chem B 104:8920
3. Khaselev O, Turner JR (1998) Science 280:425
4. Khan SUM, Akikusa J (1999) J Phys Chem B 103:7184
5. Khan SUM, Akikusa J (1998) J Electrochem Soc 145:89
6. Akikusa J, Khan SUM (1997) Int J Hydrogen Energy 22:875
7. Majumder SA, Khan SUM (1994) Int J Hydrogen Energy 19:881
8. Srivastava ON, Karn RK, Misra M (2000) Int J Hydrogen Energy 25:495
9. Bak T, Nowotny J, Rekas M, Sorrel CC (2002) Int J Hydrogen Energy 27:19
10. Akikusa J, Khan SUM (2002) Int J Hydrogen Energy 27:863
11. Yu JG, Yu HG, Cheng B, Zhao XJ, Yu JC, Ho WK (2003) J Phys Chem B 107:13871
12. Serpone N, Pelizzetti E (1989) Photocatalysis: fundamentals and applications. Wiley, New York
13. Nowotny J, Back T, Nowotny MK, Sheppard RL (2007) Int J Hydrogen Energy 32:2609
14. Mohaputra SK, Mahajan VK, Mishra M (2007) Nanotechnology 18:445705
15. Fa C, Lang LY, Weng HS (2008) Nanotechnology 19:125704
16. Xu C, Khan SUM (2007) Electrochem Solid-State Lett 10:B56
17. Xu C, Richard R, McMahan LG, Khan SUM (2006) Electrochem Commun 8:1650
18. Mohaputra SK, Mishra M, Mahajan VK (2007) J Phys Chem C 111:8677
19. Noworyta K, Augustynski J (2004) Electrochem Solid-State Lett 7:E31
20. Shaban YA, Khan SUM (2008) Int J Hydrogen Energy 33:1118
21. Shaban YA, Khan SUM (2007) Chem Phys 339:73
22. Li Y, Hwang DS, Lee NH, Kim SJ (2005) Chem Phys Lett 404:25
23. Choi W, Termin A, Hoffman MR (1994) J Phys Chem 98:13669
24. Anpo A (1997) Catal Surv Jpn 1:169
25. Choi Y, Umebayashi T, Yoshikawa M (2004) J Mater Sci 39:1837
26. Barborini E, Conti AM, Kholmanov I, Piseri P, Podesta A, Milani P, Cepek C, Sakho O, Macovez M, Sancrotti M (2005) Adv Mater 17:1842
27. Noguchi D, Kawanata Y, Nagatomo T (2005) J Electrochem Soc 152:D124
28. Xu C, Killmeyer R, Gray ML, Khan SUM (2006) Appl Catal B: Environ 64:312
29. Irie H, Watanabe Y, Hashimoto K (2003) Chem Lett 32:772
30. Sakthivel S, Kisch H (2003) Angew Chem Int Ed 42:4908
31. Asahi R, Morikawa T, Ohwaki T, Aoki K, Taga Y (2001) Science 293:269
32. Hong YC, Bang CU, Shin DH, Uhm HS (2005) Chem Phys Lett 413:454
33. Umebayashi T, Yamaki T, Itoh H, Asai K (2002) Appl Phys Lett 81:454
34. Tang J, Wu Y, McFarland W, Stucky GD (2004) Chem Commun 14:1670
35. Choi H, Stathatos E, Dionysiou DD (2006) Appl Catal B: Environ 63:60
36. Mor GK, Shankar K, Paulose M, Varghese OK, Grimes CA (2005) Nano Lett 5:191
37. Park JH, Kim S, Bard AJ (2006) Nano Lett 6:24
38. Shankar K, Paulose M, Mor GK, Varghese OK, Grimes CA (2005) J Phys D: Appl Phys 38:3543
39. Xu C, Shaban YA, Ingler WB Jr, Khan SUM (2006) ECS Trans 3:65
40. Xu C, Shaban YA, Ingler WB Jr, Khan SUM (2007) Sol Energy Mater Sol Cells 91:938
41. Hahn R, Ghicov A, Salonen J, Lehto VP, Schmuki P (2008) Nanotechnology 18:105604
42. Nakano Y, Morikawa T, Ohwaki T, Taga Y (2005) Appl Phys Lett 87:052111
43. Ren W, Ai Z, Jia F, Zhang L, Fan X, Zou Z (2007) Appl Catal B: Environ 69:138
44. Nie X, Sohlberg K (2004) Mater Res Soc Symp Proc Mater Technol Hydro Econ 801:205
45. Wang H, Lewis JP (2005) J Phys: Condens Matter 17:L209
46. Wang H, Lewis JP (2006) J Phys Condens Matter 18:421
47. Valentin CD, Pacchioni G, Selloni A (2005) Chem Mater 17:6656
48. Hägglund C, Grätzel M, Kansemo T (2003) Science 301:1673b
49. Murphy AB, Barnes PRF, Randeniya LK, Plumb IC, Grey IE, Horne MD, Glasscock JA (2006) Int J Hydrogen Energy 31:1999
50. www.nrel.gov
51. Schaller RD, Klimov VI (2004) Phys Rev Let 92:186601
52. Ellingson RJ, Beard MC, Johnson JC, Yu P, Micic OI, Nozik AJ, Shabaev A, Efros AIL (2005) Nano Lett 5:865
53. Schaller RD, Sykora M, Pietryga JM, Klimov VI (2006) Nano Lett 6:424
54. Murphy JE, Norman AJB, Ahrenkeiv AG, Yu P, Micic OI, Ellingson RJ, Norman JC, Nozik AJ (2006) J Am Chem Soc 128:3241
55. Shabaev A, Efros AIL, Nozik AJ (2006) Nano Lett 6:2856
56. Nozik AJ (2002) Physica E 14:115
57. Gleckman P, O'Gallagher J, Winston R (1989) Nature 339:198